ACS OMEGA

http://pubs.acs.org/journal/acsodf

Article

Comparative Study on the Flame Retardancy and Retarding Mechanism of Rare Earth (La, Ce, and Y)-Based Organic Frameworks on Epoxy Resin

Xiutao Li, Feng Zhang, Mengjie Zhang, Xiaomeng Zhou,* and Haijun Zhang*

Cite This: *ACS Omega* 2021, 6, 35548−35558

Read Online

ACCESS | Metrics & More | Article Recommendations | Supporting Information

ABSTRACT: In this work, a series of rare earth-based metal−organic frameworks (RE-MOFs) with the same organic ligand were synthesized and studied as flame retardants on epoxy. Through thermogravimetric analysis, limiting oxide index, UL-94, and cone calorimeter tests, a Y-based MOF (Y-MOF) showed the best flame retardancy compared with a La-based MOF (La-MOF) and Ce-based MOF (Ce-MOF). Further research with Raman, X-ray photoelectron spectroscopy, and theoretical calculation revealed that the reasons for the different flame retardance performances of RE-MOFs resulted from the catalytic carbonizing abilities and the radical-trapping abilities of La, Ce, and Y.

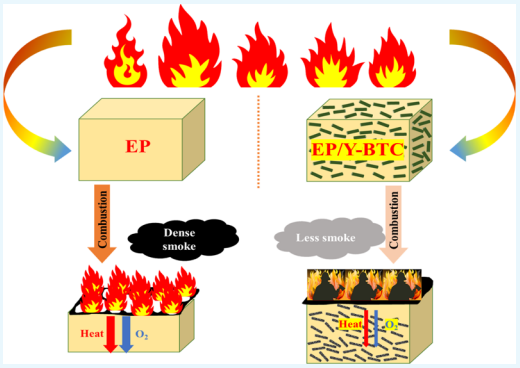

1. INTRODUCTION

Metal−organic frameworks (MOFs) are attractive crystalline porous materials that are constructed by inorganic polynuclear ions/clusters and multidentate organic linkers via coordination bonds. Due to the diverse structure, chemical tunability, and extremely high porosity, MOFs have attracted extensive interest in the past decade.[1−3] Recently, by the sheer breadth of features obtainable in the MOF field, new promises emerged for the development of novel flame retardants (FRs).[4−6] Benefiting from the organic segment of MOFs, MOF-derived FRs showed high compatibility with the polymer matrix and enhanced mechanical property of the polymer composites. Moreover, the nanoscale metal ions/clusters in MOFs play an important role in improving the FR and smoke suppression performances. Up to now, several metal centers have been selected to research the MOF-derived FRs, such as Co,[7−9] Zn,[10−12] Zr,[13−15] Al,[16,17] Fe,[18−20] Cu,[21,22] Ni,[23−25] Sn,[26] and Mo.[27] Hu et al. have found that 2D layered and 3D block MOFs combining common transition metals (such as Fe, Co, Zr, and Ni) and rigid organic complexes showed better flame retardancy with less dosage.[7−9,13,21,25] Zheng et al. reported that Co-, Zn-, and Fe-MOFs can effectively reduce the heat release rate (HRR), smoke production rate (SPR), and CO production (COP) of epoxy (EP) composites.[28] As can be seen, MOFs are potential FRs to obtain superior flame retardancy and fire safety. However, most of these MOFs have different organic ligands or crystal structures; there was no systematic study focus on the metal effect upon the flame retardancy performance. The puzzle of the metal effect will be an impediment for designing MOF-derived FRs. Thus, it is highly desirable to explore the differences of the different metal centers with similar MOF structures as FRs.

Rare-earth (RE) elements share similar chemical properties[29] and many of the RE compounds exhibit good flame retardance properties.[30−38] RE oxides or phosphates, such as lanthanum oxide,[30−34] cerium oxide/cerium phosphate,[35−37] samarium oxide,[39] and so forth, have been widely used as an effective FR synergist and smoke suppressant with the intumescent FRs in polymers. Moreover, layered double hydroxide containing Y[38] or Ce[40] elements not only facilitated the formation of the char layer achieving excellent flame retardancy and smoke suppression but also maintained favorable mechanical properties of the polymer matrix. However, there was no systematic research about RE-MOFs as FRs.

In this work, inspired by the reported flame retardancy of MOFs and RE elements, three RE-MOFs were synthesized with La, Ce, and Y as metal centers and 1,3,5-benzoic acid (BTC) as an organic ligand. The thermal decomposition and flame retardancy of RE-MOFs in the EP matrix were studied; then, an in-depth analysis was carried out to reveal the causes for the different flame retardance performances of RE-MOFs,

Received: September 15, 2021
Accepted: December 2, 2021
Published: December 16, 2021

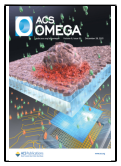

https://doi.org/10.1021/acsomega.1c05088
ACS Omega 2021, 6, 35548−35558

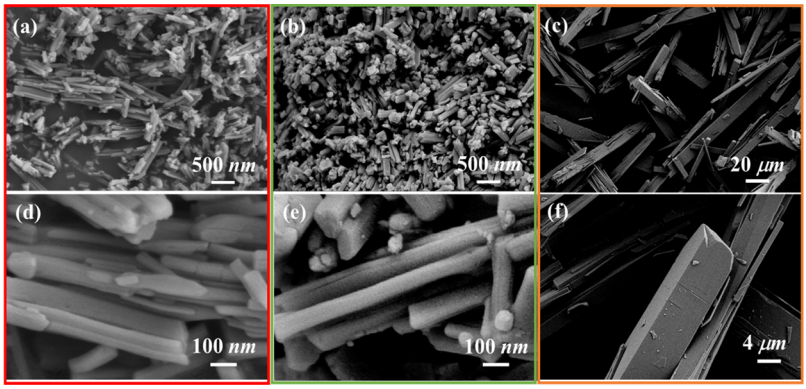

Figure 1. SEM images of (a) and (d) La-BTC, (b) and (e) Ce-BTC, and (c) and (f) Y-BTC.

and a flame-retarding mechanism was proposed. Also, the corresponding mechanical properties of RE-MOF/EP composites were researched.

2. EXPERIMENTAL SECTION

2.1. Materials. Lanthanum nitrate hexahydrate ($La(NO_3)_3 \cdot 6H_2O$), cerium nitrate hexahydrate ($Ce(NO_3)_3 \cdot 6H_2O$), and yttrium nitrate hexahydrate ($Y(NO_3)_3 \cdot 6H_2O$) were provided by Baotou Research Institute of Rare Earths. EP (E-44, epoxy equivalent = 0.44 mol/100 g) was bought from Nantong Xingchen Synthetic Material Co., Ltd. 1,4-Benzene dicarboxylic acid (BDC), 1,3,5-benzoic acid (BTC), *N*,*N*-dimethylformamide (DMF), 4,4′-diaminodiphenylmethane (DDM), and ethanol were purchased from Aladdin Chemical Reagent Co., Ltd. (Shanghai, China).

2.2. Preparation of RE-MOFs. *2.2.2. La-BTC.* In a typical process,[41] 2.165 g (5 mmol) of $La(NO_3)_3 \cdot 6H_2O$ was placed in 120 mL of deionized water and 1.051 g (5 mmol) of BTC was placed in 120 mL of water/ethanol mixture (v/v = 1:1). Then, the abovementioned two solutions were mixed at 25 °C and stirred using a magnetic stirrer for 1.5 h. Finally, the solid powder product was washed with a water/ethanol mixture (v/v = 1:1) and dried in a vacuum oven at 70 °C.

2.2.3. Ce-BTC. The preparation process of Ce-BTC was similar to La-BTC,[42] and only, 2.165 g (5 mmol) of $La(NO_3)_3 \cdot 6H_2O$ was replaced by 2.171 g (5 mmol) of $Ce(NO_3)_3 \cdot H_2O$ and the time of stirring was reduced to 10 min.

2.2.4. Y-BTC. As a typical preparation procedure,[43] 1.915 g (5 mmol) of $Y(NO_3)_3 \cdot 6H_2O$ and 1.051 g (5 mmol) of BTC were dissolved in 120 mL of DMF/water mixture (v/v = 5:1), followed by magnetic stirring until the mixture was fully dissolved. Then, the mixture was transferred to a conical flask and kept at 100 °C for 12 h. Finally, the product was washed with water and ethanol, respectively, and dried in a vacuum oven at 70 °C.

2.3. Preparation of EP and EP/RE-MOF Composites. EP/RE-MOF composites were prepared using a facile solution blending method. First, 4 wt % as-prepared RE-MOFs were ultrasonically dispersed in a suitable amount of acetone until completely dispersed. Subsequently, the dispersion solution was added into EP and stirred at 90 °C for 2 h. Next, the hardener DDM (ratio of EP/DDM was 10:3) was poured into the abovementioned solution and stirred for 5 min. Finally, the mixture was transferred into the customized Teflon mold, followed by curing at 110, 130, and 150 °C for 2 h, respectively. The pure EP without adding RE-MOFs underwent the same process. Samples with La-BTC, Ce-BTC, and Y-BTC were labeled EP/La-BTC, EP/Ce-BTC, and EP/Y-BTC, respectively.

2.4. Characterization. The morphology of the samples was observed on a ZEISS Gemini 300 scanning electron microscope (Germany) at an acceleration voltage of 10 kV. The Brunauer−Emmett−Teller (BET) surface area and porous structures were analyzed based on N_2 adsorption−desorption isotherms using an ASAP 2460 (Micromeritics Instrument Corp., USA). X-ray diffraction (XRD) was performed on an Ultima IV instrument (Rigaku, Japan) using Cu Kα radiation (40 kV and 100 mA) in the 2θ range from 10 to 80° with a scan rate of 5° min^{-1}. Thermogravimetric analysis (TGA) was carried out on a TGA 701 instrument (LECO, USA) under N_2 conditions with a ramping rate of 10 °C/min. X-ray photoelectron spectroscopy (XPS) was carried out in a Thermo Scientific Escalab 250 Xi spectrometer equipped with a monochromatic Al Kα X-ray source ($h\nu$ = 1486.6 eV). All XP spectra were recorded using an aperture slot measuring 300 μm × 700 μm. Survey and high-resolution spectra recorded with pass energies (within ±0.2 eV) were determined, with respect to the position of the adventitious C 1s peak at 284.6 eV. Raman spectroscopy was performed with a CRM 2000 laser Raman spectrometer (Renishaw, UK) using a 514 nm laser. The fire behavior was studied using a cone calorimeter test (CCT) (FTT, UK) according to ISO 5660, and the samples (100 × 100 × 4 mm^3) were irradiated at a heat flux of 50 $kW \cdot m^{-2}$. The limiting oxide index (LOI) was tested using a JF-6 Automatic Oxygen Indexer (Jiangning Analytical Instruments, China) according to ASTM D2863, and the sheet dimensions were 100 × 10 × 3 mm^3. UL-94 (vertical burning test) was carried on a CZF-5 instrument according to ASTM D3801 with sample dimensions of 130 × 13 × 3 mm^3. The tensile properties were tested on a WDW-10M electronic testing machine (Jinan Zhongluchang Instrument, China) according to ISO178 under a rate of 2 mm/min.

2.5. Computation. All the first-principles computations were carried out by employing the projector-augmented plane wave[44,45] method as implemented in the Vienna Ab inito Simulation Package (VASP)[46,47] code. The electron exchange−correlation functional was described by the generalized gradient approximation in the form proposed by Perdew, Burke, and Ernzerhof.[48] The tolerance for energy convergence was set to 10^{-5} eV, while the ionic relaxation is converged when the force on each atom was less than 10^{-3} eV/Å. The 550 eV cutoff for a plane-wave basis set was adopted in all computations. The Brillouin zone was integrated using

https://doi.org/10.1021/acsomega.1c05088
ACS Omega 2021, 6, 35548−35558

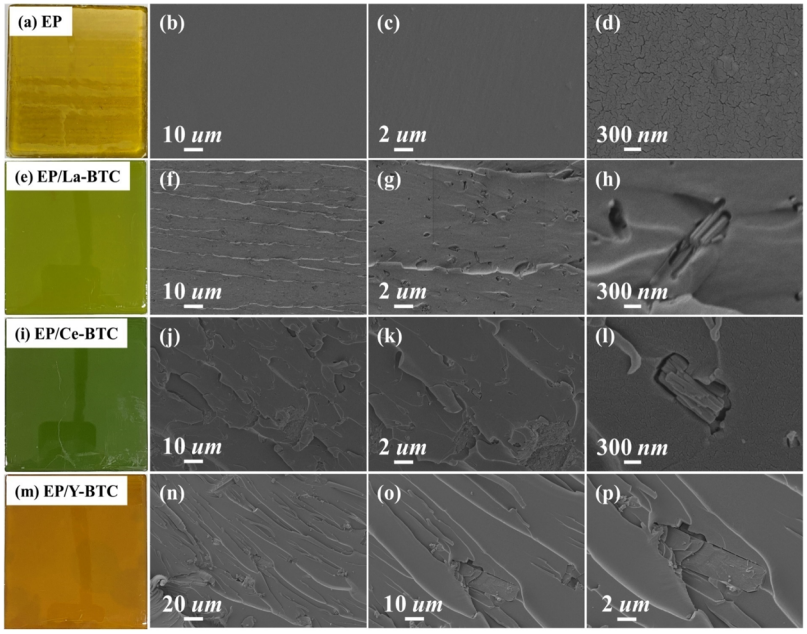

Figure 2. Digital photographs of (a) EP, (e) EP/La-BTC, (i) EP/Ce-BTC, and (m) EP/Y-BTC and SEM images of brittle rupture surfaces of (b–d) EP, (f–h) EP/La-BTC, (j–l) EP/Ce-BTC, and (n–p) EP/Y-BTC.

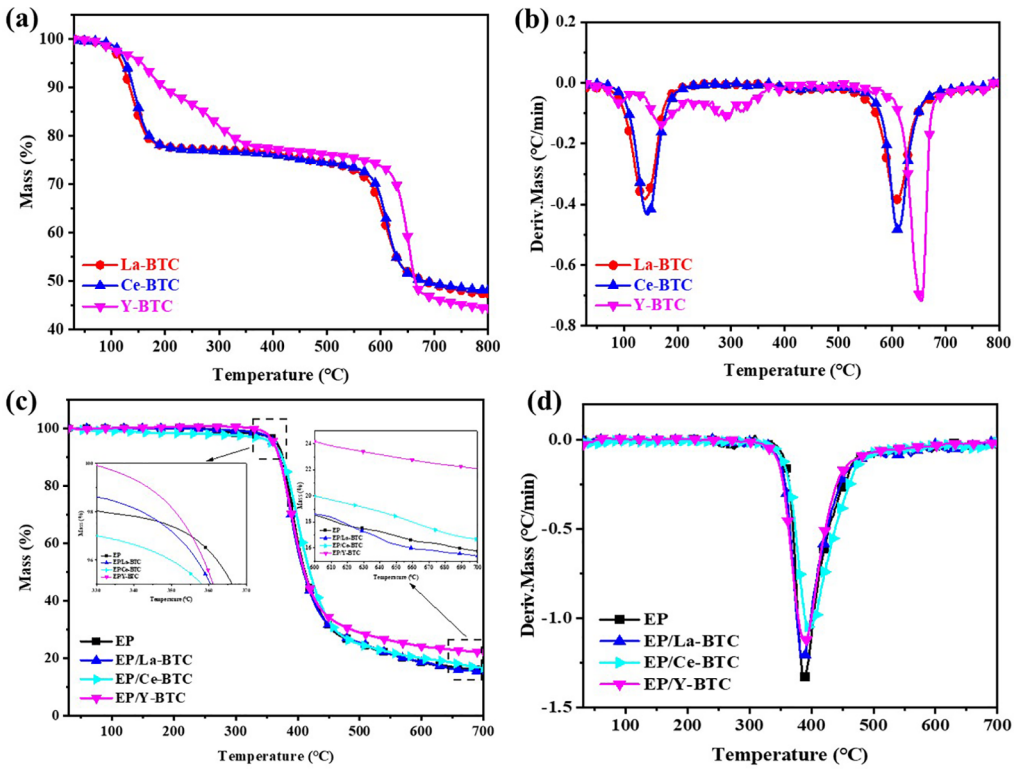

Figure 3. TG/DTG curves of RE-MOFs (a,b) and EP and EP/RE-MOFs (c,d) under N_2 conditions.

Monkhorst–Pack-generated sets of *k*-points. In the geometry relaxation and self-consistent computations, 7 × 7 × 1 Monkhorst–Pack *k*-point mesh was used.

3. RESULTS AND DISCUSSION

3.1. Characterization of RE-MOFs and EP Composites.

RE-MOFs were prepared according to the previous reports, and their crystal structures were confirmed by XRD patterns, as illustrated in Figure S1. For La-BTC and Ce-BTC, both of them have similar characteristic diffraction peaks in the range of 5–50°, which can be well-indexed to a bulk phase of La(BTC) $(H_2O)_6$[49] and Ce(BTC)$(H_2O)_6$,[42] respectively. With regard to Y-BTC, the strong and narrow diffraction peaks (2θ = 8.6, 10.6, 18.3, and 20.3°) show excellent agreement with the XRD pattern of simulated Y(BTC) (H_2O) $(DMF)_{1.1}$.[43] The morphologies of the RE-MOF crystals were characterized by SEM images, as shown in Figure 1. It can be seen the shapes of all RE-MOFs are rod-shaped crystals, but

https://doi.org/10.1021/acsomega.1c05088
ACS Omega 2021, 6, 35548–35558

compared with La-BTC and Ce-BTC, Y-BTC shows a more regular morphology and larger size. Besides, the porous features of RE-MOFs were studied by N_2 physisorption experiments (Figure S2 ad Table S1). The specific surface areas of La-MOF, Ce-MOF, and Y-MOF are 22.18, 16.39, and 2.11 m^2/g, respectively, which are very close to the previously reported values (17.3 m^2/g for La-MOF,[50−52] 13.0 m^2/g for Ce-MOF,[53,54] and 10.0 m^2/g for Y-MOF[54,55]). The above-mentioned characterizations demonstrate the successful synthesis of RE-MOFs.

It is well-known that the dispersion degree of FRs in polymer plays an important role in the FR efficiency of the matrix. From the digital photographs of EP and EP composites (Figure 2a,e,i,m), it can be seen that the EP/RE-MOF samples are quite well-distributed on the macroscale. The micro-distributions of RE-MOFs in EP were studied by SEM images of the brittle rupture surfaces. As can be seen, compared with the smooth fracture surface of pure EP (Figure 2b−d), EP/RE-MOFs showed rather rough and ribbed structural surfaces (Figure 2f−h,j−l,n−p). The multirib structures may help us to enhance the mechanical properties of the EP matrix. Moreover, most of the RE-MOFs were embedded in EP and there was no obvious aggregation, which indicates that there were well distribution and good interaction between RE-MOFs and the EP matrix.

3.2. Thermal Property and Flame Retardancy.

3.2.1. Thermal Properties of RE-MOFs and EP Composites. Thermal stabilities of the obtained RE-MOFs were studied by TGA. From Figure 3a,b, it can be seen that all the RE-MOFs showed two degradation stages, the first degradation stage (100−300 °C) is corresponding to the volatilization of solvent molecules (H_2O or DMF) and the second degradation stage (550−700 °C) is due to the decomposition of the organic groups and MOF structures. Compared with La-BTC and Ce-BTC, Y-BTC exhibited a better thermal stability, which may attribute to its structural integrity upon exposure to heat, vacuum, or pressure treatment.[56]

The thermal degradation behavior of neat EP and its composites were also measured by TGA, and the corresponding TG/DTG curves are portrayed in Figure 3c,d. The related data including the initial decomposition temperature (calculated as 5%, $T_{5\%}$) and the char residue are listed in Table 1. It

Table 1. Data of TGA and DTG of Pure EP and EP Composites

		char yield (%)			
samples	$T_{5\%}$ (°C)	550 °C	600 °C	650 °C	700 °C
EP	366.1	21.4	18.5	16.9	15.8
EP/La-BTC	360.0	21.5	18.6	16.3	15.4
EP/Ce-BTC	358.1	22.0	20.0	18.4	16.7
EP/Y-BTC	360.7	26.1	24.1	22.9	22.1

can be observed that the $T_{5\%}$ of EP/RE-MOFs composites is slightly delayed, suggesting that the incorporation of RE-MOFs can give rise to earlier initial degradation of EP composites, which is due to the catalytic decomposition effect of MOFs.[57] The char residue is an important characteristic for the flame retardancy of polymers; generally, the higher the char yield, the better the flame retardancy. TGA results clearly show that the addition of Y-BTC can significantly increase the char yield of EP, while the addition of La-BTC or Ce-BTC has no apparent effect, which means that Y-BTC may have better flame retardancy than La-BTC and Ce-BTC.

3.2.2. Flame Retardancy and Smoke Suppression of EP and Its Composites. The fire safeties of EP composites were first evaluated by LOI measurements and UL-94 vertical burning test. The LOI is the maximum oxygen concentration required to support candle-like combustion in a given testing time and is an important parameter for characterizing the flammability of the polymer materials. As can be seen from Figure 4, compared with pure EP, the LOI values of EP/RE-MOF composites all increased, especially for EP/Y-BTC, which is up to 29%. Moreover, for EP, the dropping phenomenon occurred and the flammable drops ignited the cotton (Figure 4b), while the addition of Y-BTC effectively inhibited the melt dropping of EP (Figure 4c), which can reduce the risk of secondary injury in a fire. These results show that Y-BTC could endow excellent flame retardancy to EP.

The combustion behaviors of all samples were further investigated using the CCT, which can simulate bench-scale fire including the release of heat, smoke, suffocating gas (CO and CO_2), and so forth. From Figure 5a, it can be seen that the incorporation of the RE-MOF results in almost no change in the shape of the HRR profiles. However, the highest peak of the HRRs (pHRR) of the EP/RE-MOF composites is reduced in comparison with the pure EP, and the decreasing trend is Y-BTC (28.2%) > Ce-BTC (1.7%) > La-BTC (−2.7%). A similar decreasing trend of the THR values is also observed for the EP/RE-MOF composites, which is Y-BTC (12.7%) > Ce-BTC (−3.2%) > La-BTC (−6.9%) (Figure 5b and Table 2). Furthermore, the char yields of EP/RE-MOF composites have an increasing trend as Y-BTC (120.1%) > Ce-BTC (11.4%) > La-BTC (−15.8%) (Figure 5c and Table 2). To more clearly assess the fire hazards and the performance of flame retardancy of EP/RE-MOF composites, the fire growth index (FGI) and flame retardancy index (FRI) were calculated according to the following equations

$$\mathrm{FGI} = \frac{\mathrm{pHRR}}{t\text{-pHRR}} \tag{1}$$

$$\mathrm{FRI} = \frac{\mathrm{THR}^{*}\left(\frac{\mathrm{pHRR}}{\mathrm{TTI}}\right)_{\text{neat polymers}}}{\mathrm{THR}^{*}\left(\frac{\mathrm{pHRR}}{\mathrm{TTI}}\right)_{\text{composites}}} \tag{2}$$

where *t*-pHRR represents the time to pHRR and TTI represents the time to ignition. The values of *t*-pHRR and TTI are listed in Table 2. Generally, with a lower FGI or higher FRI value, EP composites get better fire safety.[58] The value of FGI follows the sequence of EP/Ce-BTC (9.42) > EP/La-BTC (9.01) > EP (8.43) > EP/Y-BTC (6.58), and the value of FRI follows the sequence of EP/La-BTC (0.78) < EP/Ce-BTC (0.92) < EP (1.00) < EP/Y-BTC (1.37). All the abovementioned results indicate that Y-BTC has the most positive effect on the flame retardancy of EP, while La-BTC and Ce-BTC almost have no FR effect on EP.

It is well-known that the released smoke during combustion processes is another significant factor for accessing the fire safety of polymers. From Figure 6 and Table 2, it is clear that only Y-BTC can effectively reduce the release of the peak of SPR (pSPR) and total smoke production (TSP) at the same time, which is consistent with the results of pHRR and THR. Compared with pure EP, the EP/Y-BTC composite manifests the most effective smoke suppression effect, and the values of

https://doi.org/10.1021/acsomega.1c05088
ACS Omega 2021, 6, 35548−35558

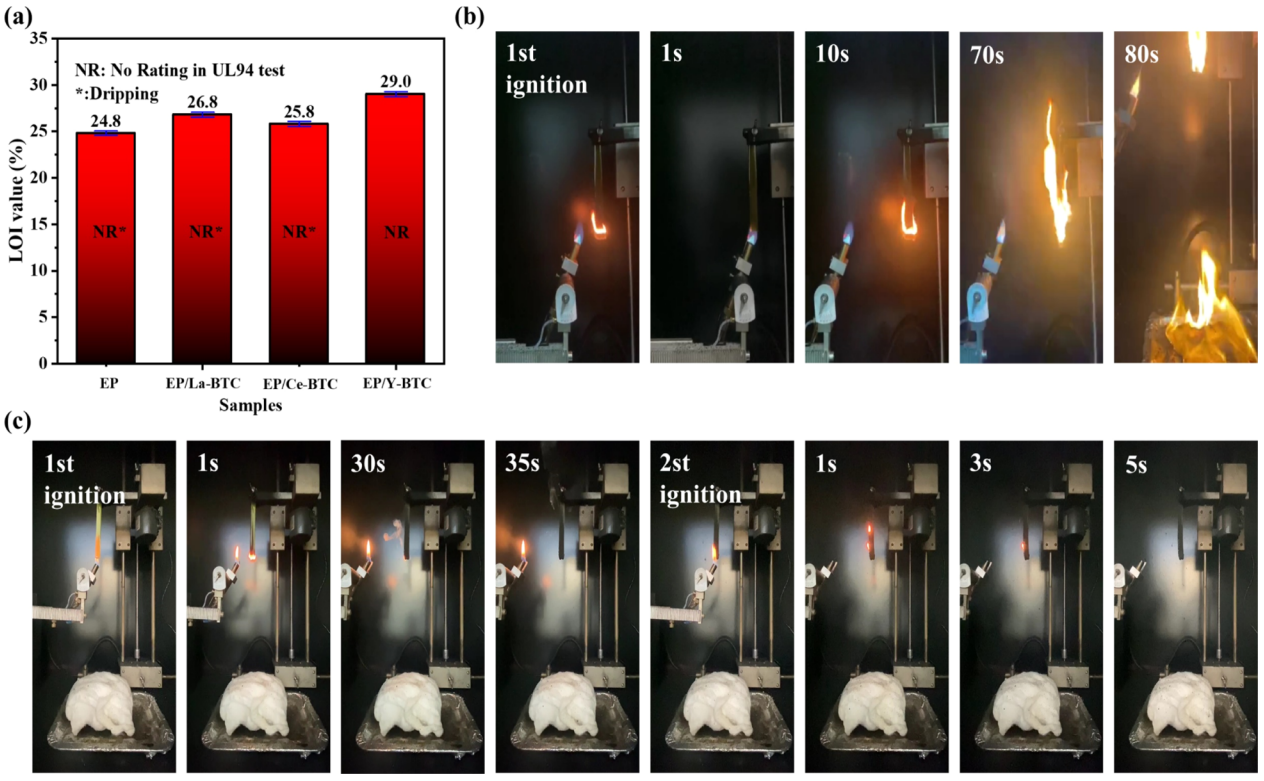

Figure 4. (a) LOI and UL-94 data of EP composites and digital photographs of EP (b) and EP/Y-BTC (c) during the UL-94 vertical burning test process.

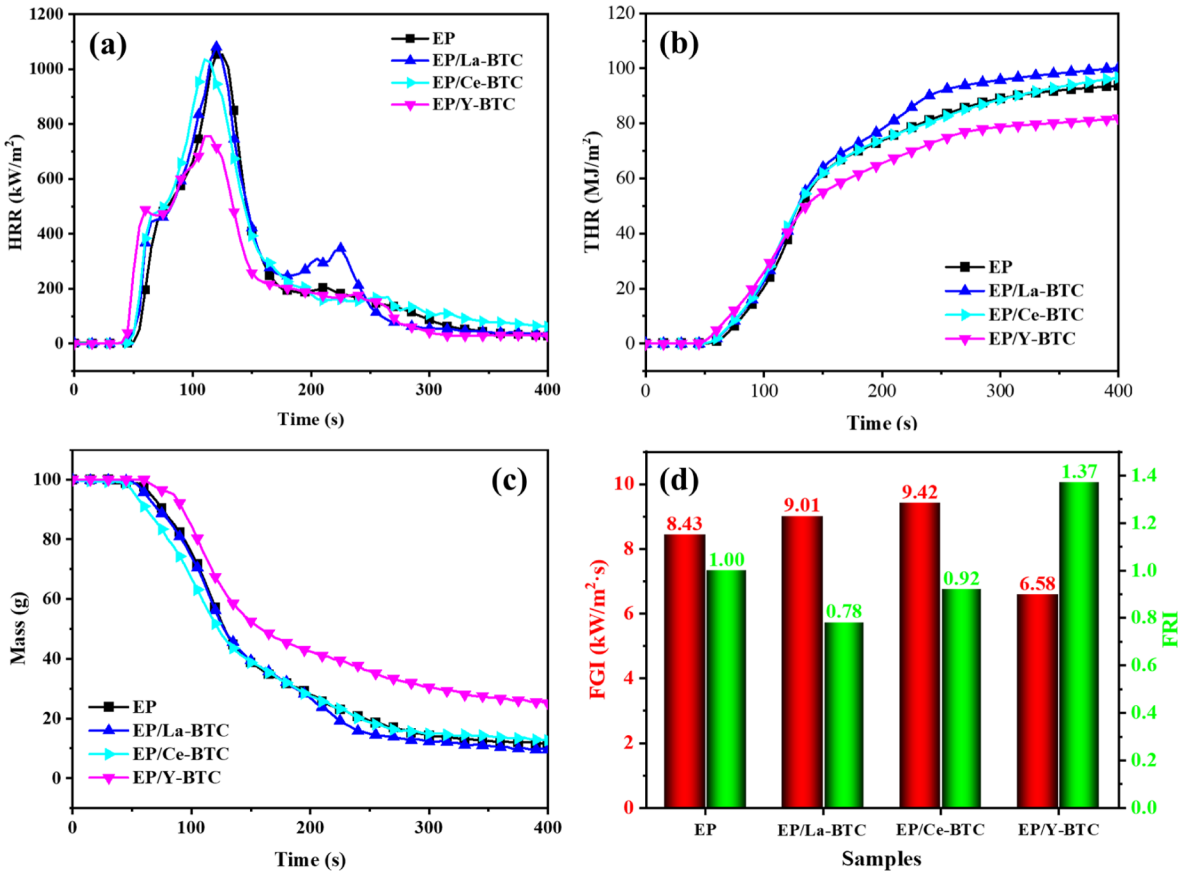

Figure 5. HRR (a), THR (b), char yield (c) curves, and FGI and FPI values (d) of neat EP and EP/RE-MOF composites.

https://doi.org/10.1021/acsomega.1c05088
ACS Omega 2021, 6, 35548−35558

Table 2. Parameters about Heat, Smoke, and Suffocating Gas in CCT of EP and Its Composites

category	parameter	EP	EP/La-BTC	EP/Ce-BTC	EP/Y-BTC
heat	TTI (s)	43	37	40	37
	pHRR (kW/m^2)	1053.3	1081.4	1035.9	756.7
	t-pHRR (s)	125	120	110	115
	THR (MJ/m^2)	93.7	100.2	96.7	81.8
	residues (wt %)	11.4	9.6	12.7	25.1
smoke	pSEA (m^2/kg)	3918.6	2225.4	3429.9	1434.8
	aSEA (m^2/kg)	761.5	741.0	752.8	719.7
	pSPR (m^2/s)	0.266	0.290	0.248	0.211
	TSP (m^2)	28.2	30.1	28.4	23.9
suffocating gas	pCOP (g/s)	0.030	0.032	0.027	0.021
	pCO$_2$P (g/s)	0.559	0.661	0.598	0.459
	TCO (g)	2.297	2.565	2.192	2.023
	TCO$_2$ (g)	60.80	67.40	64.35	54.50

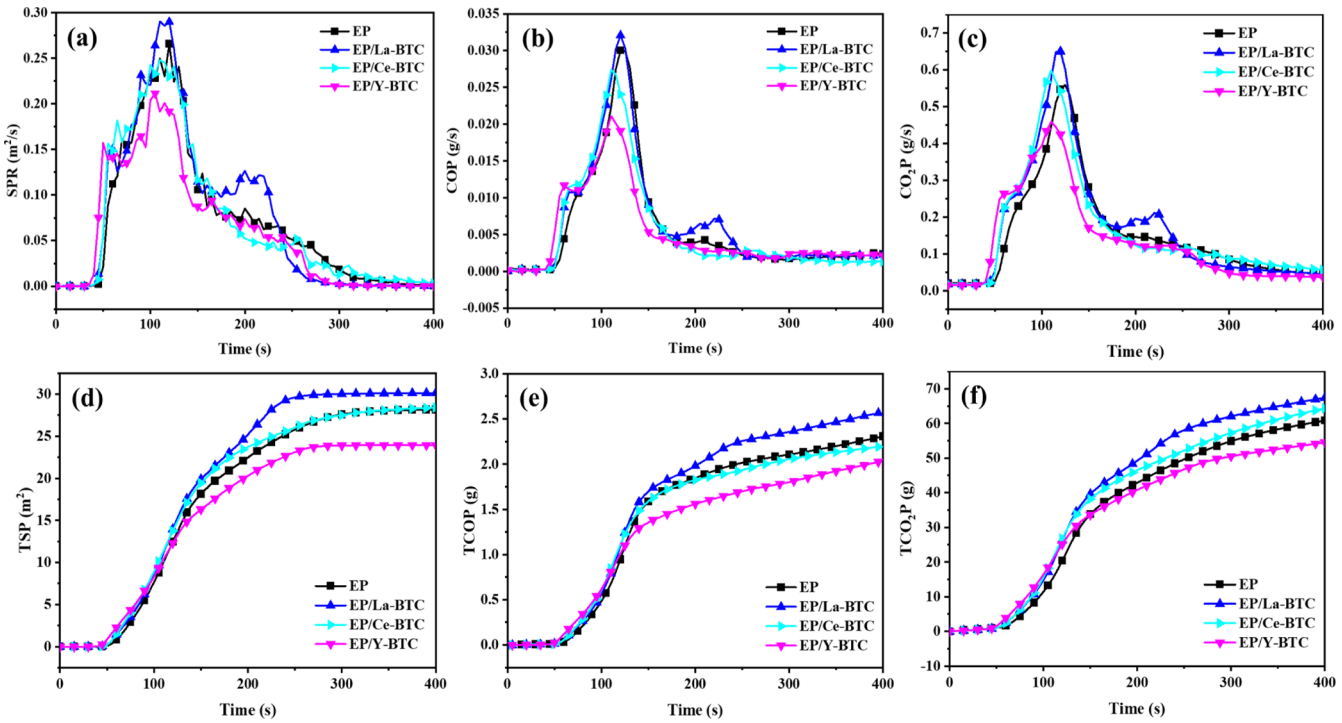

Figure 6. SPR (a), COP (b), CO_2P (c), TSP (d), TCOP (e), and TCO_2p (f) curves of neat EP and EP/RE-MOF composites.

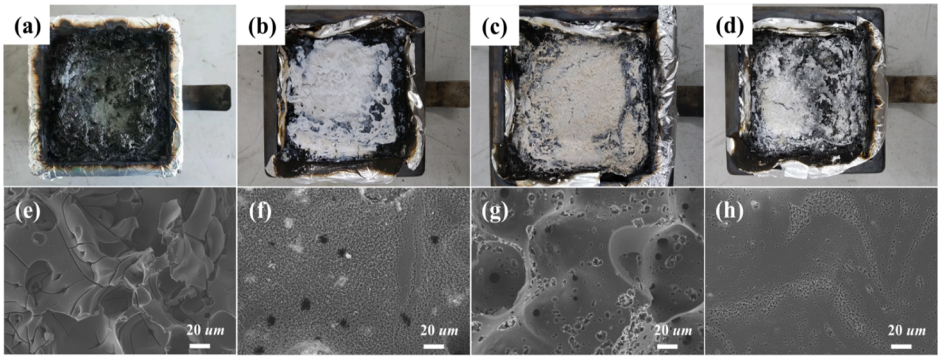

Figure 7. Digital and SEM images of the char residues of the samples after the CCT: EP (a,e), EP/La-BTC (b,f), EP/Ce-BTC (c,g), and EP/Y-BTC (d,h).

pSPR and TSP were reduced by 20.1 and 15.2%, respectively. Moreover, for the EP/Y-BTC composite, another important factor describing the flow rate of combustible gas, the specific extinction area (SEA), also showed a great reduction. For instance, the peak of SEA (pSEA) and the average of SEA (aSEA) were reduced by 63.4 and 5.5%, respectively (Table 2).

https://doi.org/10.1021/acsomega.1c05088
ACS Omega 2021, 6, 35548−35558

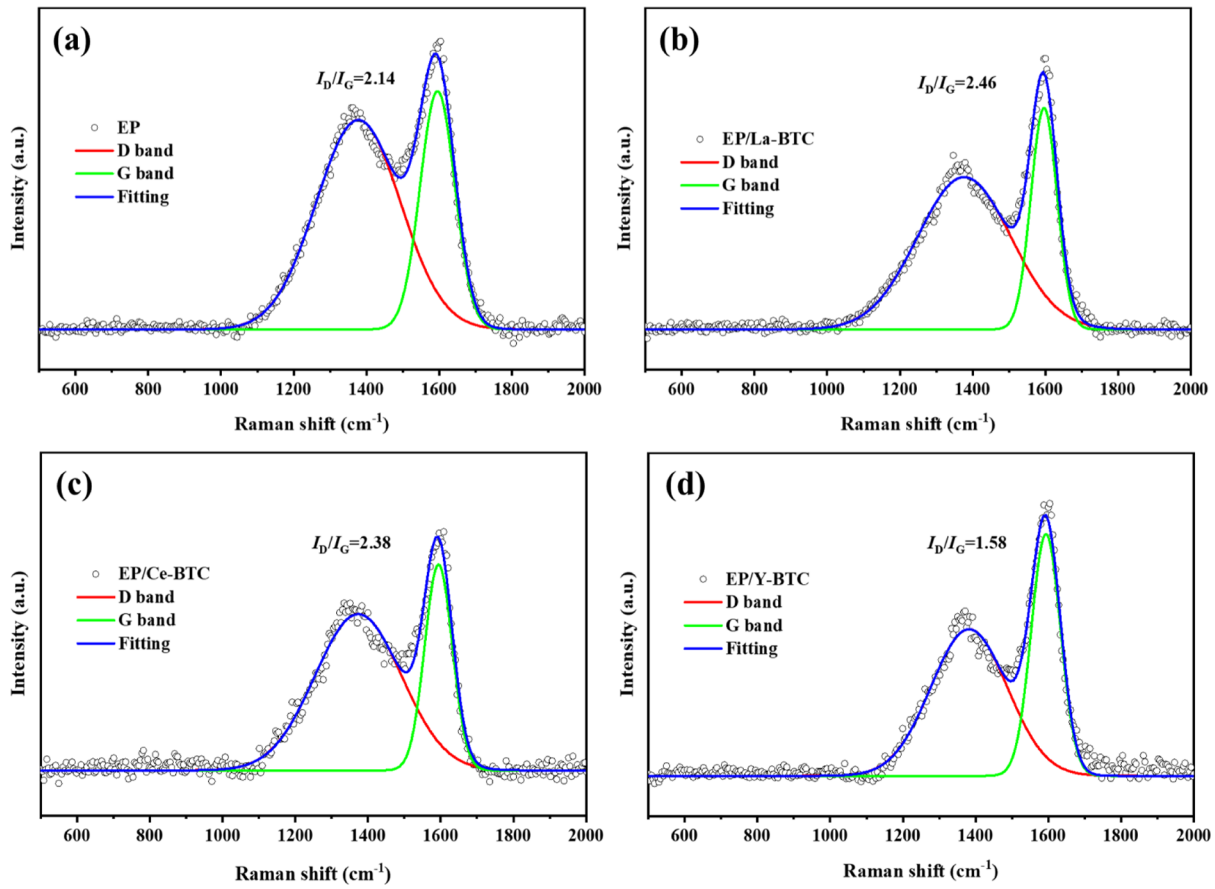

Figure 8. Raman spectra of the char residues of the samples after the CCT: EP (a), EP/La-BTC (b), EP/Ce-BTC (c), and EP/Y-BTC (d).

Furthermore, the toxicity gas CO generation of the EP/Y-BTC composite was decreased significantly. As can be seen from Table 2, the peak of CO production (pCOP) and total CO production (TCOP) were decreased by 30.0 and 11.9%, respectively, in comparison with those of neat EP. However, compared with Y-BTC, La-BTC and Ce-BTC exhibited no or very weak smoke and CO suppression capability.

Based on these analyses, we can conclude that Y-BTC not only presents a high heat-release suppression performance but also exhibits a strong smoke, CO, and CO_2 suppression ability. Moreover, compared with the previously reported MOF FRs (such as Cu-MOF, Co-MOF, Zn-MOF, Fe-MOF, Sn-MOF, Zr-MOF, Al-MOF, Mo-MOF, and Ni-MOF, as shown in Table S2), Y-BTC prepared in this work showed a better comprehensive performance.

3.3. FR Mechanism Analysis. *3.3.1. Catalytic Carbonizing Abilities of RE Compounds.* To analyze the effect of the FR on the char formation, the digital photographs and SEM images of the char residues after the CCT were studied (as shown in Figure 7). From Figure 7a−d, it can be seen that the neat EP almost burns out, resulting in very little char residue with a fragmentary structure, and the EP/La-BTC composite shows loose char residues with a lot of holes on the surface; however, an almost integrated residue was formed both for Ce-BTC and Y-BTC. Furthermore, the SEM images reveal that the residue produced by EP is porous and unconsolidated (Figure 7e); for EP/La-BTC and EP/Ce-BTC, although there are still a few holes, the residues are relatively integrated (Figure 7f,g), while for the EP/Y-BTC, the char layer becomes intact and compact, which can act as a protective barrier in suppressing flame transfer (Figure 7h).

The graphitization degree is an important parameter to measure the stability of the char residue, which can be characterized by Raman. As shown in Figure 8, the D and G bands at 1350 and 1600 cm^{-1} are corresponding to the peak of amorphous and graphitized carbon, respectively, and the ratio of the D and G band intensity (I_D/I_G) is used for evaluating the degree of graphitization. It can be seen that the trend of I_D/I_G is EP/La-BTC (2.46) > EP/Ce-BTC (2.38) > EP (2.14) > EP/Y-BTC (1.58), which indicates that the char residue produced by EP/Y-BTC has the highest degree of graphitization. According to the previous reports about MOF carbonization, MOFs with different metals would form different graphitic degree carbons[27,59−61] and the graphitic degree is determined by the catalytic carbonizing effect of metals. Thus, the high graphitization degree of EP/Y-BTC may be due to the high catalytic carbonizing abilities of Y.

The chemical structures of EP and its composites were further investigated by XPS analysis to study the thermal oxidative resistance of polymers. It can be found from Figure S3 that the C 1s XPS spectra of all samples could be fitted into three sub-bands at 284.8, 286.0, and 288.8 eV, which are assigned to C−C (aliphatic and aromatic species, represented as C_a), C−O (ether and/or hydroxyl species, represented as C_{ox}), and C═O (carbonyl and/or carboxyl species, represented as C_{ox}), respectively.[27] Generally, the smaller the C_{ox}/C_a ratio, the stronger the thermal oxidation resistance of the char residues. In combination with Figure S2 and Table 3, it is clear that the C_{ox}/C_a values of EP/RE-MOFs are in the

https://doi.org/10.1021/acsomega.1c05088
ACS Omega 2021, 6, 35548−35558

Table 3. XPS Data of the Char Residues of the Samples after the CCT

	area (%)			
samples	C 1s (C−C)	C 1s (C−O)	C 1s (C═O)	C_{ox}/C_a ratio
EP	64.12	30.87	5.01	0.60
EP/La-BTC	60.50	33.67	5.83	0.65
EP/Ce-BTC	69.61	15.31	15.08	0.44
EP/Y-BTC	75.34	11.40	13.26	0.33

order of EP/La-BTC (0.65) > EP (0.60) > EP/Ce-BTC (0.44) > EP/Y-BTC (0.33), which indicates that Y-BTC would enhance the thermal oxidation stability of the char layer more availably. This result is consistent with that of the Raman analysis.

3.3.2. Radical Trapping Abilities of RE Compounds. From the abovementioned discussion, we can conclude that compared with La-BTC and Ce-BTC, the excellent FR effect of Y-BTC is benefitted from the high stable carbon formation ability of Y which can prevent the heat transfer and the flame spread. In fact, the thermal degradation of the polymer is a free-radical chain reaction; the radical-trapping ability is also an important factor in reducing the flammability of the polymer.[62] Besides, it was found that the OH• radical plays an important role in the whole thermal oxygen degradation mechanism of the polymer.[63] Thus, the adsorption energy of OH• on the final RE compounds that have direct contact with the flame can be used to evaluate the FR performance. In this work, a computational method was employed to assess the capability of capturing the OH• radical for La, Ce, and Y. According to the XRD analysis of the char residues of the samples after the CCT (Figure S4), the final RE compounds in EP/RE-MOFs were Y_2O_3, CeO_2, and La_2CO_5, respectively. It should be noted that the La_2O_3 generated during EP/La-BTC combustion will be transferred to La_2CO_5 when exposed to atmospheric CO_2.[64] Thus, the slab models of Y_2O_3(222) facets, CeO_2(111) facets, and La_2CO_5(001) facets were constructed to simulate different exposed facets of RE compounds. The OH• group absorbed on the Y_2O_3(222) facets, CeO_2(111) facets, and La_2CO_5(001) facets were completely optimized to the lowest-energy structures, as shown in Figure 9.

The adsorption energy (E_{ad}) was defined as $E_{ad} = E_T - (E_{slab} + E_{group})$. Accordingly, the smaller adsorption energy indicates the energetically preferable adsorption of free radicals on RE compounds. The calculated adsorption energies of OH• on Y_2O_3, CeO_2, and La_2CO_5 materials were 0.79, 1.34, and 2.19 eV, respectively. The lowest E_{ad} of the Y_2O_3 surface implies the highest capability of Y_2O_3 for capturing the OH• radicals. Additionally, the greatest E_{ad} of OH• adsorbed on La_2CO_5 suggests the most unfavorability of the adsorption and thus the poorest capability of capturing radicals. As can be seen, the high radical-trapping ability of Y is another important factor for the excellent flame retardance, since it can block the degradation process of EP.

3.3.3. Proposed Mechanism. Based on the abovementioned discussion and analysis, it is interesting to observe that the addition of Y-BTC has the most efficient effect on reducing the heat radiation and suppressing the smoke release, and a possible mechanism is proposed, as shown in Figure 10. For the pure EP, it is easy to absorb heat and release pyrolysis products without limitation under the action of heating. Large amounts of heat, dense smoke, toxic volatile gases, and suffocating gases (CO and CO_2) are released in the case of fire. However, the addition of Y-BTC significantly inhibited the release of a large amount of heat, smoke, and toxic volatile gases, which can be explained by the following reasons. On the one hand, during the pyrolysis process of EP/Y-BTC composites, Y may catalyze the formation of the char layer. The char layer with a superior graphitization degree and better oxidation resistance can be functioned as a barrier to prevent the transfer of heat and decomposition products. On the other hand, the formed Y_2O_3 can trap the free radicals in the chain reaction and block the degradation process of EP.

3.4. Mechanical Properties of EP and Its Composites.

It is well-known that the incorporation of FRs will influence the mechanical properties of the EP matrix. The mechanical performance of EP and its composites was investigated by tensile tests. Figure 11 shows the stress−strain curves of EP and its composites and their mechanical parameters, including tensile strength (σ) and elongation at break (ε). The σ and ε of neat EP can reach about 53.06 MPa and 10.31%, respectively. The addition of La-BTC was slightly averse to the mechanical performance of EP. Different from La-BTC, although the values of EP/Ce-BTC and EP/Y-BTC decreased, their σ values were slightly improved by 7.5 and 1.8%, respectively. In other words, the addition of Ce-BTC and Y-BTC can enhance the EP's tensile strength but decrease the elongation performance. The tensile strength enhancement may result from the formed multirib structure (as shown in Figure 2). The decrease in elongation may be due to the small amounts of pores produced during preparation, which can be removed by improving the preparation method.

4. CONCLUSIONS

In this work, three similar RE-MOFs constructed with La, Ce, and Y as metal centers and BTC as an organic ligand were examined as FRs for EP composites. Comprehensive TGA, LOI, UL-94, and CCT results indicated that compared with La-BTC and Ce-BTC, Y-BTC observably enhanced the thermostability and flame retardancy of the EP composites. According to the Raman and XPS analysis of char residues of EP and its composites, the higher catalytic carbonizing effect of

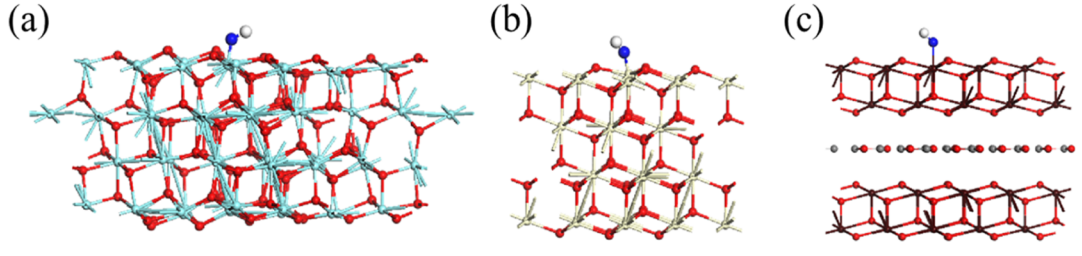

Figure 9. Optimized geometries of the OH• group absorbed on the (a) Y_2O_3(222), (b) CeO_2(111), and (c) La_2CO_5(001) facets.

https://doi.org/10.1021/acsomega.1c05088
ACS Omega 2021, 6, 35548−35558

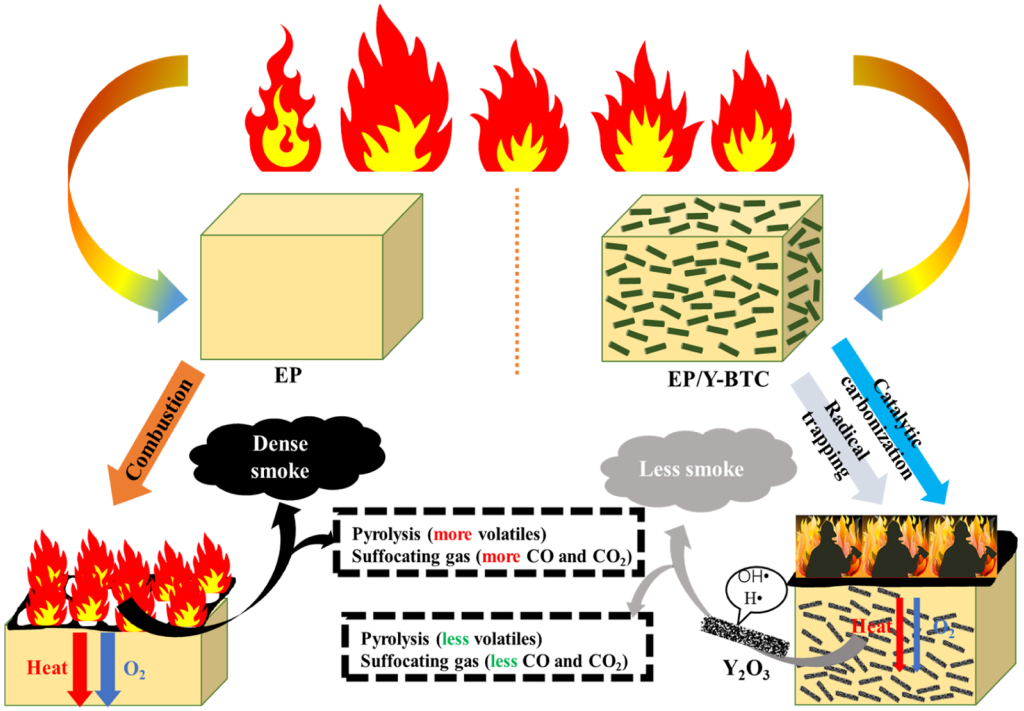

Figure 10. Schematic illustration of the proposed mechanism of EP/Y-BTC.

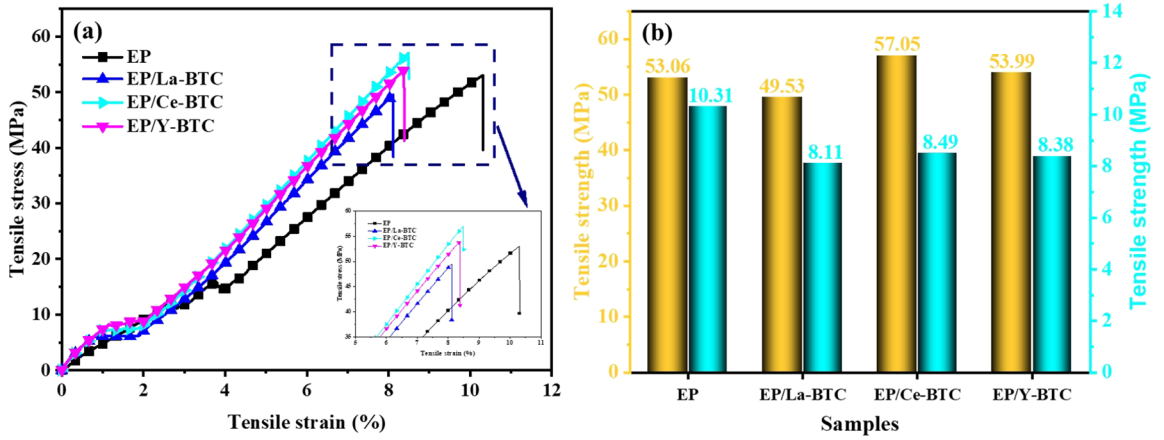

Figure 11. Tensile stress−strain curves (a) and tensile strength and elongation at break (b) of EP and its composites.

Y can substantially improve the graphitization degree and oxidation resistance of the char layer which enhances the flame retardance of Y-BTC. Furthermore, the higher free-radical-trapping ability of Y_2O_3 may be another contribution to the flame retardance, which can block the chain reaction of EP degradation. Based on the study of this work, the catalytic carbonizing ability and free-radical-trapping ability of the metal center in the MOF should be focused on the design and development of MOF-derived retardants in the future. In addition, the effects of organic ligands and MOF structures on the abovementioned properties will be studied in our next work.

■ ASSOCIATED CONTENT

Supporting Information

The Supporting Information is available free of charge at https://pubs.acs.org/doi/10.1021/acsomega.1c05088.

XRD patterns and N_2 adsorption−desorption isotherms of RE-MOFs, high-resolution C 1s XPS spectra and XRD spectra of the char residues of the samples, and performance comparisons of MOF-based FRs in polymer composites (PDF)

■ AUTHOR INFORMATION

Corresponding Authors

Xiaomeng Zhou − *Key Laboratory of Civil Aviation Thermal Hazards Prevention and Emergency Response, Civil Aviation University of China, Tianjin 300300, China;* orcid.org/0000-0003-1258-9935; Email: zhouxm@nankai.edu.cn

Haijun Zhang − *Key Laboratory of Civil Aviation Thermal Hazards Prevention and Emergency Response, Civil Aviation University of China, Tianjin 300300, China;* orcid.org/0000-0002-9082-3662; Email: hjzhang_ahu@163.com

https://doi.org/10.1021/acsomega.1c05088
ACS Omega 2021, 6, 35548−35558

Authors

Xiutao Li − *Key Laboratory of Civil Aviation Thermal Hazards Prevention and Emergency Response, Civil Aviation University of China, Tianjin 300300, China*

Feng Zhang − *Key Laboratory of Civil Aviation Thermal Hazards Prevention and Emergency Response, Civil Aviation University of China, Tianjin 300300, China*

Mengjie Zhang − *Key Laboratory of Civil Aviation Thermal Hazards Prevention and Emergency Response, Civil Aviation University of China, Tianjin 300300, China*

Complete contact information is available at: https://pubs.acs.org/10.1021/acsomega.1c05088

Author Contributions

All authors equally contributed to this work.

Notes

The authors declare no competing financial interest.

■ ACKNOWLEDGMENTS

This work was supported by the Fundamental Research Funds for the Central Universities (no. 3122021064).

■ REFERENCES

(1) Furukawa, H.; Cordova, K. E.; O'Keeffe, M.; Yaghi, O. M. The Chemistry and Applications of Metal-Organic Frameworks. *Science* **2013**, *341*, 1230444.

(2) Lee, J.; Farha, O. K.; Roberts, J.; Scheidt, K. A.; Nguyen, S. T.; Hupp, J. T. Metal-organic framework materials as catalysts. *Chem. Soc. Rev.* **2009**, *38*, 1450−1459.

(3) Li, J.-R.; Kuppler, R. J.; Zhou, H.-C. Selective gas adsorption and separation in metal-organic frameworks. *Chem. Soc. Rev.* **2009**, *38*, 1477−1504.

(4) Nabipour, H.; Wang, X.; Song, L.; Hu, Y. Metal-organic frameworks for flame retardant polymers application: A critical review. *Composites, Part A* **2020**, *139*, 106113.

(5) Zhang, J.; Li, Z.; Qi, X. L.; Wang, D. Y. Recent Progress on Metal-Organic Framework and Its Derivatives as Novel Fire Retardants to Polymeric Materials. *Nano-Micro Lett.* **2020**, *12*, 173.

(6) Pan, Y.-T.; Zhang, Z. D.; Yang, R. J. The rise of MOFs and their derivatives for flame retardant polymeric materials: A critical review. *Composites, Part B* **2020**, *199*, 108265.

(7) Hou, Y.; Hu, W.; Gui, Z.; Hu, Y. Preparation of Metal-Organic Frameworks and Their Application as Flame Retardants for Polystyrene. *Ind. Eng. Chem. Res.* **2017**, *56*, 2036−2045.

(8) Hou, Y.; Hu, W.; Gui, Z.; Hu, Y. A novel Co(II)-based metal-organic framework with phosphorus-containing structure: Build for enhancing fire safety of epoxy. *Compos. Sci. Technol.* **2017**, *152*, 231−242.

(9) Xu, Z.; Xing, W.; Hou, Y.; Zou, B.; Han, L.; Hu, W.; Hu, Y. The combustion and pyrolysis process of flame-retardant polystyrene/cobalt-based metal organic frameworks (MOF) nanocomposite. *Combust. Flame* **2021**, *226*, 108−116.

(10) Shi, X.; Dai, X.; Cao, Y.; Li, J.; Huo, C.; Wang, X. Degradable Poly(lactic acid)/Metal−Organic Framework Nanocomposites Exhibiting Good Mechanical, Flame Retardant, and Dielectric Properties for the Fabrication of Disposable Electronics. *Ind. Eng. Chem. Res.* **2017**, *56*, 3887−3894.

(11) Zhao, S.; Yin, L.; Zhou, Q.; Liu, C.; Zhou, K. In situ self-assembly of zeolitic imidazolate frameworks on the surface of flexible polyurethane foam: Towards for highly efficient oil spill cleanup and fire safety. *Appl. Surf. Sci.* **2020**, *506*, 144700.

(12) Cheng, J.; Ma, D.; Li, S. X.; Qu, W. J.; Wang, D. Preparation of Zeolitic Imidazolate Frameworks and Their Application as Flame Retardant and Smoke Suppression Agent for Rigid Polyurethane Foams. *Polymers* **2020**, *12*, 347.

(13) Chen, W.; Jiang, Y.; Qiu, R.; Xu, W.; Hou, Y. Investigation of UiO-66 as Flame Retardant and Its Application in Improving Fire Safety of Polystyrene. *Macromol. Res.* **2020**, *28*, 42−50.

(14) Sai, T.; Ran, S. Y.; Guo, Z. H.; Fang, Z. P. A Zr-based metal organic frameworks towards improving fire safety and thermal stability of polycarbonate. *Composites, Part B* **2019**, *176*, 107198.

(15) Zhang, J.; Li, Z.; Zhang, L.; Yang, Y.; Wang, D.-Y. Green Synthesis of Biomass Phytic Acid-Functionalized UiO-66-NH_2 Hierarchical Hybrids toward Fire Safety of Epoxy Resin. *ACS Sustainable Chem. Eng.* **2020**, *8*, 994−1003.

(16) Huang, R.; Guo, X. Y.; Ma, S. Y.; Xie, J. X.; Xu, J. Z.; Ma, J. Novel Phosphorus-Nitrogen-Containing Ionic Liquid Modified Metal-Organic Framework as an Effective Flame Retardant for Epoxy Resin. *Polymers* **2020**, *12*, 108.

(17) Wang, J.; Liu, Y.; Guo, X.; Qu, H.; Chang, R.; Ma, J. Efficient Adsorption of Dyes Using Polyethyleneimine-Modified NH_2-MIL-101(Al) and its Sustainable Application as a Flame Retardant for an Epoxy Resin. *ACS Omega* **2020**, *5*, 32286−32294.

(18) Sang, L.; Cheng, Y.; Yang, R.; Li, J.; Kong, Q.; Zhang, J. Polyphosphazene-wrapped Fe-MOF for improving flame retardancy and smoke suppression of epoxy resins. *J. Therm. Anal. Calorim.* **2021**, *144*, 51−59.

(19) Chen, Z.; Chen, T.; Yu, Y.; Zhang, Q.; Chen, Z.; Jiang, J. Metal-organic framework MIL-53 (Fe)@C/graphite carbon nitride hybrids with enhanced thermal stability, flame retardancy, and smoke suppression for unsaturated polyester resin. *Polym. Adv. Technol.* **2019**, *30*, 2458−2467.

(20) Li, Y.; Li, X.; Pan, Y.; Xu, X.; Song, Y.; Yang, R. Mitigation the release of toxic PH_3 and the fire hazard of PA6/AHP composite by MOFs. *J. Hazard. Mater.* **2020**, *395*, 122604.

(21) Hou, Y.; Chu, F.; Ma, S.; Hu, Y.; Hu, W.; Gui, Z. Rapid Synthesis of Oxygen-Rich Covalent C_2N (CNO) Nanosheets by Sacrifice of HKUST-1: Advanced Metal-Free Nanofillers for Polymers. *ACS Appl. Mater. Interfaces* **2018**, *10*, 32688−32697.

(22) Qi, X.-L.; Zhou, D.-D.; Zhang, J.; Hu, S.; Haranczyk, M.; Wang, D.-Y. Simultaneous Improvement of Mechanical and Fire-Safety Properties of Polymer Composites with Phosphonate-Loaded MOF Additives. *ACS Appl. Mater. Interfaces* **2019**, *11*, 20325−20332.

(23) Zhang, L.; Chen, S.; Pan, Y.-T.; Zhang, S.; Nie, S.; Wei, P.; Zhang, X.; Wang, R.; Wang, D.-Y. Nickel Metal-Organic Framework Derived Hierarchically Mesoporous Nickel Phosphate toward Smoke Suppression and Mechanical Enhancement of Intumescent Flame Retardant Wood Fiber/Poly(lactic acid) Composites. *ACS Sustainable Chem. Eng.* **2019**, *7*, 9272−9280.

(24) Wang, X.; Wang, S.; Wang, W.; Li, H.; Liu, X.; Gu, X.; Bourbigot, S.; Wang, Z. W.; Sun, J.; Zhang, S. The flammability and mechanical properties of poly (lactic acid) composites containing Ni-MOF nanosheets with polyhydroxy groups. *Composites, Part B* **2020**, *183*, 107568.

(25) Hou, Y.; Hu, W.; Zhou, X.; Gui, Z.; Hu, Y. Vertically Aligned Nickel 2-Methylimidazole Metal-Organic Framework Fabricated from Graphene Oxides for Enhancing Fire Safety of Polystyrene. *Ind. Eng. Chem. Res.* **2017**, *56*, 8778−8786.

(26) Ma, S.; Hou, Y.; Xiao, Y.; Chu, F. K.; Cai, T. M.; Hu, W. Z.; Hu, Y. Metal-organic framework@polyaniline nanoarchitecture for improved fire safety and mechanical performance of epoxy resin. *Mater. Chem. Phys.* **2020**, *247*, 122875.

(27) Zhang, F.; Li, X.; Yang, L.; Zhang, Y.; Zhang, M. A Mo-based metal-organic framework toward improving flame retardancy and smoke suppression of epoxy resin. *Polym. Adv. Technol.* **2021**, *32*, 3266−3277.

(28) Zheng, Y.; Lu, Y.; Zhou, K. A novel exploration of metal−organic frameworks in flame-retardant epoxy composites. *J. Therm. Anal. Calorim.* **2019**, *138*, 905.

(29) Liang, T.; Ding, S.; Song, W.; Chong, Z.; Zhang, C.; Li, H. A review of fractionations of rare earth elements in plants. *J. Rare Earths* **2008**, *26*, 7−15.

(30) Li, Y.; Li, B.; Dai, J.; Jia, H.; Gao, S. Synergistic effects of lanthanum oxide on a novel intumescent flame retardant polypropylene system. *Polym. Degrad. Stab.* **2008**, *93*, 9−16.
(31) Jing Wu, J.; Yuan Hu, Y.; Lei Song, L.; Wenjie Kang, W. J. Synergistic effect of lanthanum oxide on intumescent flame-retardant polypropylene-based formulations. *J. Fire Sci.* **2008**, *26*, 399−414.
(32) Song, L.; Zhou, S.; Wu, J.; Hu, Y. Synergistic Effects of Lanthanum Oxide on Magnesium Hydroxide Flame-Retarded Ethylene Propylene Diene Terpolymer Composite. *Polym.-Plast. Technol. Eng.* **2009**, *48*, 1088−1093.
(33) Wang, L.; Yang, W.; Wang, B.; Wu, Y.; Hu, Y.; Song, L.; Yuen, R. K. K. The Impact of Metal Oxides on the Combustion Behavior of Ethylene-Vinyl Acetate Coploymers Containing an Intumenscent Flame Retardant. *Ind. Eng. Chem. Res.* **2012**, *51*, 7884−7890.
(34) Feng, C.; Liang, M.; Zhang, Y.; Jiang, J.; Huang, J.; Liu, H. Synergistic effect of lanthanum oxide on the flame retardant properties and mechanism of an intumescent flame retardant PLA composites. *J. Anal. Appl. Pyrolysis* **2016**, *122*, 241−248.
(35) Qiao, Z.; Tai, Q.; Song, L.; Hu, Y.; Lv, P.; Jie, G.; Huang, W.; Fu, Y.; Zhang, D. Synergistic effects of cerium phosphate and intumescent flame retardant on EPDM/PP composites. *Polym. Adv. Technol.* **2011**, *22*, 2602−2608.
(36) Li, J.; Liu, G. Flame retardancy properties of ammonium polyphosphate with crystalline form II by non-P_2O_5 process. *Polym. Degrad. Stab.* **2012**, *97*, 2562−2566.
(37) Feng, C.; Liang, M.; Jiang, J.; zhang, Y.; Huang, J.; Liu, H. Synergism effect of CeO_2 on the flame retardant performance of intumescent flame retardant polypropylene composites and its mechanism. *J. Anal. Appl. Pyrolysis* **2016**, *122*, 405−414.
(38) Qian, Y.; Han, H.; Li, L.; Qiao, P.; Zhao, R.; Zhang, H. Combustion behavior and thermal stability of TPU composites based on layered yttrium hydroxides and graphene oxide. *J. Therm. Anal. Calorim.* **2020**, *142*, 409−423.
(39) Zhang, H.; Lu, X.; Zhang, Y. Synergistic effects of rare earth oxides on intumescent flame retardancy of Nylon 1010/ethylene-vinyl-acetate rubber thermoplastic elastomers. *J. Polym. Res.* **2015**, *22*, 10.
(40) Liu, Y.; Li, B.; Xu, M.; Wang, L. Highly Efficient Composite Flame Retardants for Improving the Flame Retardancy, Thermal Stability, Smoke Suppression, and Mechanical Properties of EVA. *Materials* **2020**, *13*, 1251.
(41) Afzal, S.; Quan, X.; Zhang, J. High surface area mesoporous nanocast LaMO 3 (M = Mn, Fe) perovskites for efficient catalytic ozonation and an insight into probable catalytic mechanism. *Appl. Catal., B* **2017**, *206*, 692−703.
(42) Liu, K.; You, H.; Jia, G.; Zheng, Y.; Huang, Y.; Song, Y.; Yang, M.; Zhang, L.; Zhang, H. Hierarchically Nanostructured Coordination Polymer: Facile and Rapid Fabrication and Tunable Morphologies. *Cryst. Growth Des.* **2010**, *10*, 790−797.
(43) Jiang, H.-L.; Tsumori, N.; Xu, Q. A series of (6,6)-connected porous lanthanideorganic framework enantiomers with high thermostability and exposed metal sites: scalable syntheses, structures, and sorption properties. *Inorg. Chem.* **2010**, *49*, 10001−10006.
(44) Blöchl, P. E. Projector augmented-wave method. *Phys. Rev. B: Condens. Matter Mater. Phys.* **1994**, *50*, 17953−17979.
(45) Kresse, G.; Joubert, D. From ultrasoft pseudopotentials to the projector augmented-wave method. *Phys. Rev. B* **1999**, *59*, 1758−1775.
(46) Kresse, G.; Hafner, J. Ab initio molecular dynamics for open-shell transition metals. *Phys. Rev. B: Condens. Matter Mater. Phys.* **1993**, *48*, 13115−13118.
(47) Kresse, G.; Furthmüller, J. Efficient iterative schemes for ab initio total-energy calculations using a plane-wave basis set. *Phys. Rev. B: Condens. Matter Mater. Phys.* **1996**, *54*, 11169−11186.
(48) Perdew, J. P.; Burke, K.; Ernzerhof, M. Generalized Gradient Approximation Made Simple. *Phys. Rev. Lett.* **1996**, *77*, 3865−3868.
(49) Liu, K.; Zheng, Y.; Jia, G.; Yang, M.; Song, Y.; Guo, N.; You, H. Nano/micro-scaled La(1,3,5-BTC)$(H_2O)_6$ coordination polymer: Facile morphology-controlled fabrication and color-tunable photoluminescence properties by co-doping Eu^{3+}, Tb^{3+}. *J. Solid State Chem.* **2010**, *183*, 2309−2316.
(50) Liu, J.-W.; Zhang, Y.; Chen, X.-W.; Wang, J.-H. Graphene Oxide-Rare Earth Metal-Organic Framework Composites for the Selective Isolation of Hemoglobin. *ACS Appl. Mater. Interfaces* **2014**, *6*, 10196−10204.
(51) Shang, W.; Kang, X.; Ning, H.; Zhang, J.; Zhang, X.; Wu, Z.; Mo, G.; Xing, X.; Han, B. Shape and Size Controlled Synthesis of MOF Nanocrystals with the Assistance of Ionic Liquid Mircoemulsions. *Langmuir* **2013**, *29*, 13168−13174.
(52) Zhang, X.; Sun, F.; He, J.; Xu, H.; Cui, F.; Wang, W. Robust phosphate capture over inorganic adsorbents derived from lanthanum metal organic frameworks. *Chem. Eng. J.* **2017**, *326*, 1086−1094.
(53) Chen, G.; Guo, Z.; Zhao, W.; Gao, D.; Li, C.; Ye, C.; Sun, G. Design of Porous/Hollow Structured Ceria by Partial Thermal Decomposition of Ce-MOF and Selective Etching. *ACS Appl. Mater. Interfaces* **2017**, *9*, 39594−39601.
(54) Huang, Z.; Zhao, F.; Fan, L.; Zhao, W.; Chen, B.; Chen, X.; Zhou, S.; Xiao, J.; Zhan, G. Improved hydrolytic robustness and catalytic performance of flexible lanthanide-based metal-organic frameworks: A matter of coordination environments. *Mater. Des.* **2020**, *194*, 108881.
(55) Shu, Y.; Meng, Y.; Chen, M.-L.; Wang, J.-H. Isolation of hemoglobin with metal-organic frameworks Y(BTC)$(H_2O)_6$. *Chin. Chem. Lett.* **2015**, *26*, 1460−1464.
(56) Ding, M.; Cai, X.; Jiang, H.-L. Improving MOF stability: approaches and applications. *Chem. Sci.* **2019**, *10*, 10209−10230.
(57) Xu, B.; Xu, W.; Wang, G.; Liu, L.; Xu, J. Zeolitic imidazolate frameworks-8 modified graphene as a green flame retardant for reducing the fire risk of epoxy resin. *Polym. Adv. Technol.* **2018**, *29*, 1733−1743.
(58) Yan, Y.-W.; Chen, L.; Jian, R.-K.; Kong, S.; Wang, Y.-Z. Intumescence: An effect way to flame retardance and smoke suppression for polystryene. *Polym. Degrad. Stab.* **2012**, *97*, 1423−1431.
(59) Li, L.; Dai, P.; Gu, X.; Wang, Y.; Yan, L.; Zhao, X. High oxygen reduction activity on a metal−organic framework derived carbon combined with high degree of graphitization and pyridinic-N dopants. *J. Mater. Chem. A* **2017**, *5*, 789−795.
(60) Tang, J.; Salunkhe, R. R.; Zhang, H.; Malgras, V.; Ahamad, T.; Alshehri, S. M.; Kobayashi, N.; Tominaka, S.; Ide, Y.; Kim, J. H.; Yamauchi, Y. Bimetallic Metal-Organic Frameworks for Controlled Catalytic Graphitization of Nanoporous Carbons. *Sci. Rep.* **2016**, *6*, 30295.
(61) Yang, L.; Zeng, X.; Wang, W.; Cao, D. Recent Progress in MOF-Derived, Heteroatom-Doped Porous Carbons as Highly Efficient Electrocatalysts for Oxygen Reduction Reaction in Fuel Cells. *Adv. Funct. Mater.* **2018**, *28*, 1704537.
(62) Ran, S.; Zhao, L.; Han, L.; Guo, Z.; Fang, Z. Improvement of the thermal and thermo-oxidative stability of high-density polyethylene by free radical trapping of rare earth compound. *Thermochim. Acta* **2015**, *612*, 55−62.
(63) Achimsky, L.; Audouin, L.; Verdu, J. Kinetic study of the thermal oxidation of polypropylene. *Polym. Degrad. Stab.* **1997**, *57*, 231−240.
(64) Bernal, S.; Diaz, J.; Garcia, R.; Rodriguez-Izquierdo. Study of some aspects of the reactivity of La_2O_3 with CO_2 and H_2O. *J. Mater. Sci.* **1985**, *20*, 537−541.

https://doi.org/10.1021/acsomega.1c05088
ACS Omega 2021, 6, 35548−35558